Modeling of Synthetic Fiber Ropes and Frequency Response of Long-Distance Cable–Pulley System

Atsushi Takata [ID], Gen Endo [ID], *Member, IEEE*, Koichi Suzumori, *Member, IEEE*,
Hiroyuki Nabae [ID], *Member, IEEE*, Yoshihiro Mizutani, and Yoshiro Suzuki [ID]

Abstract—In recent years, synthetic fiber ropes have attracted much attention because of their potential to increase the load capacity, reduce the size, and lighten the weight of tendon-driven mechanisms. However, the mechanical characteristics of synthetic fiber ropes in a dynamic loading situation remain an open problem because of their visco-elasto-plasticity. This letter focuses on modeling synthetic fiber ropes, and the frequency response of a long-distance cable–pulley system for a tendon-driven robot. We show that a synthetic fiber rope can be modeled by Flory's model, and that it can be reduced to a conventional four-element model with sufficient preloading. After empirically acquiring the parameters of the four-element model for four different synthetic fiber ropes, each frequency response of a long-distance cable–pulley servo system was measured and compared to the analytical results based on the model, as well as the results of a stainless wire rope. Consequently, we show that synthetic fiber ropes achieved comparable bandwidth to that of the stainless wire rope. The damping of synthetic fiber ropes was found to suppress the servo system gain. This is useful for joint control of a tendon-driven robot with a relatively large amount of inertia, such as a long-reach robot arm.

Index Terms—Tendon/wire mechanism, synthetic fiber ropes, frequency response, mechanism design.

I. INTRODUCTION

TENDON-DRIVEN mechanisms provide light, simple, and long-distance transmission more easily than other transmission mechanisms such as gears and link mechanisms. Recently, synthetic fiber ropes have been developed that are lightweight and as strong or stronger than stainless steel wire ropes [1]–[3] as shown in Table I. They have attracted attention in tendon-driven robotics, because synthetic fiber ropes can be expected to realize tendon-driven mechanisms with a higher load capacity, smaller size, and lighter weight. For example, a cable robot was designed to use a lightweight rope to save energy [4], and a quadruped walking robot [5] and a human mimetic humanoid [6] were developed by exploiting the small bending radius of synthetic fiber ropes. Moreover, an articulated long-reach robot arm exceeding 10 m in length driven by cable-pulley

TABLE I
PROPERTIES OF ROPES 2 MM IN DIAMETER

Name	Model	Supplier	Tensile strength [kN]	Weight [g/m]	Fiber	Structure
Dyneema2	DB-96HSL*	Hayami industry	4.29	2.4	Dyneema® SK-71 UHPE	2640 dtex × 8 strand braid
Zylon2	ZB-308*	Hayami industry	6.59	2.9	Zylon® AS PBO	3340 dtex × 8 strand braid
Vectran2	VB-308*	Hayami industry	4.18	2.9	Vectran® HT Polyarylate	3340 dtex × 8 strand braid
Kevlar2	KB-308*	Hayami industry	4.08	3.0	Kevlar® 29 Para-aramid	3340 dtex × 8 strand braid
Stainless1	SC-200	SHINYO	3.56	16.3	SUS304	7×19

* without preload

systems is required to decommission the Fukushima Daiichi Nuclear Power Station [7].

However, there is a difficulty to develop robots taking advantage of synthetic fiber ropes. We do not have design guidelines for synthetic fiber ropes because their characteristics have not been comprehensively studied. Our ultimate goal is to establish design guidelines for tendon-driven mechanisms using the ropes. To fulfill the design guidelines, we need to investigate the various physical properties of synthetic fiber ropes. Tensile strength, creep elongation, and repetitive bending durability are of course important for designing robots.

In this particular paper, we focused on modeling the characteristics of synthetic fiber ropes and the frequency response of a long-distance cable-pulley system. Although synthetic fiber ropes have high strength, it is generally known that synthetic fiber ropes engender more elongation than stainless cables. Given that stainless cables are simple and elastic, the mechanical behavior of synthetic fiber ropes shows visco-elasto-plasticity. For example, one of our previous works reported that the stiffness of synthetic fiber ropes was strongly affected by consecutive impact loading [8]. Thus, the dynamic behavior of a mechanism using synthetic fiber ropes is also expected to be complicated. Moreover, the mechanical properties of tendons influence the dynamic characteristics of the mechanism, depending on the length of a tendon. The question is whether the bandwidth of a servo system using synthetic fiber ropes is lower than that of a system using stainless cables. Therefore, the purpose of this letter is to model synthetic fiber ropes and investigate the frequency response of a cable-pulley system as a most general tendon-driven servo mechanism.
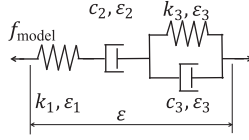
Fig. 1. Four-element model [14].

Fig. 2. Flory's model [15].

Many robotics studies have dealt with tensile elongation of tendons. For instance, [9] analyzed one servo winch system assuming that it is a second-order lag system, and improved the absolute positional accuracy of a cable-driven parallel robot. Moreover, [10] used a black box model to describe the hysteresis effect of a cable. Mazumdar *et al.* [11] presented a compact and lightweight capstan drive mechanism using a synthetic fiber rope. However, these studies focused on limited types of ropes. To the best of our knowledge, there has been no comprehensive study on the relationship between the mechanical properties of ropes and the dynamic characteristics of the mechanism. This letter is a groundwork for tendon-driven robots using synthetic fiber ropes. We verified a previously proposed model for a mooring rope. The frequency response of a 15 m long cable-pulley system was investigated using rope models and measurements.

This letter is structured as follows. In Section II, an existing model for mooring ropes is introduced. On the basis of two tensile tests, the model was verified to be applicable to the small diameter synthetic fiber ropes used for robots. In Section III, the visco-elasticity of ropes was measured. The parameters for visco-elasticity were estimated by fitting the tension relaxation, and quantitatively compared with the others. In Section IV, we used a cable-pulley servo mechanism to measure the dynamic characteristics of the mechanism, applying different types of ropes. In Section V, we discuss the visco-elasticity of the ropes, along with the frequency response of the servo mechanism and relationships between them. In Section VI, conclusions and future work are provided.

II. FLORY'S MODEL

There have been many studies on the visco-elasto-plasticity of synthetic fiber ropes used for mooring. For example, some studies predicted the elongation of mooring ropes occurring over an extremely long time by using a nonlinear function of time and stress [12], [13]. On the other hand, Flory separated the behavior of synthetic fiber ropes into nonlinear elasto-plasticity and linear visco-elasticity. He expressed the nonlinear elasto-plasticity by using a parallel element of a ratchet and spring. The parallel element were combined with a four-element model [14, Fig. 1] to propose his model [15, Fig. 2].

The four-element model is often used for linear visco-elasticity. This model considers visco-elasticity as a combination of element representing elasticity, viscosity and retarded elasticity, and separates the total strain into strains of each elements. Each element in Fig. 1 are explained as follows. The leftmost spring represents elasticity. The dashpot in the middle represents viscosity or creep. The rightmost parallel element of the spring and dashpot represents retarded elasticity. f_{model}[N] is the tension, k_1 and k_3[N] are the elastic coefficients per strain, c_2 and c_3[N $\cdot$ s] are the viscosity coefficients per strain. These parameters are normalized by length because they are inversely proportional to length, but they are not nominalized by area because a real cross sectional area of ropes is difficult to
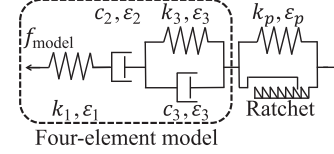
measure and the nominal diameter of ropes in this letter is 2 mm. Here, ε is the total strain. ε_1, ε_2 and ε_3 are the strains of the corresponding elements.

The Flory's model contains the four-element model explained above. k_p is the elastic coefficient per strain of the spring parallel to the ratchet element in Fig. 2. If the mechanical properties are assumed to follow the Flory's model, two relations can be expected between the tension and strain at loading and unloading.

First, when tension is applied to the parallel elements of the spring and ratchet, plastic strain occurs. Because the ratchet element suppresses shrinkage, the plastic strain retains the value at the maximum tension applied previously. The strain at maximum tension f_{peak} is defined as $\varepsilon_{\mathrm{peak}}$, a plastic strain remaining after unloading is ε_p and a elastic strain recovered after unloading is ε_1. In order to further increase the parallel elements, it is necessary to add a tension that exceeds the previous maximum tension f_{peak}. Conversely, as long as the tension of the Flory's model is subsequently lower, the plastic strain ε_p does not increase. In that case, the Flory's model can be considered as the four-element model shown in Fig. 1.

Second, if the loading speed is sufficiently high and the strain caused by the viscosity is ignored, the relations between the load and strain can be represented as follows:

$$\varepsilon_{\mathrm{peak}} = \varepsilon_1 + \varepsilon_p, \tag{1}$$

$$f_{\mathrm{peak}} = k_1 \varepsilon_1 = k_p \varepsilon_p. \tag{2}$$

Therefore, maximum tension f_{peak} increases in proportion to ε_p and ε_1 respectively. Considering these relations, the properties of synthetic fiber ropes become linear by a high preload. This is expected to provide high bandwidth and linearity to a cable-pulley servo using synthetic fiber ropes.

However, mooring ropes are more than 10 mm in diameter with loads of several hundred kilonewtons, whereas the ropes used in many robotic applications are thin with diameters of about 0.5 mm to 5 mm. For example, a rope of 1.6 mm in diameter was used for a humanoid [6], and 6 mm rope was used for a parallel wire robot [4]. Because of the differences in the scale of the load and the number of strands, the model of previous studies cannot be directly applied to this study without verification. Table I lists the types of rope used in this letter, namely, four synthetic fiber ropes and one stainless steel wire rope. Experiments were performed to verify whether the two relations of the synthetic fiber ropes hold, and to confirm whether the Flory's model can be applied.

A. Convergence of the Plastic Strain at Maximum Tension

A cyclic load test was performed on ropes in this letter. If the Flory's model is applicable for the test rope, the plastic strain will not increase as long as the loading tension does not exceed the maximum tension applied in the past. The test ropes were repeatedly pulled five times with a 10 mm/min stroke

Stroke speed	10 mm/min
Maximum load	1000 N
Minimum load	5 N
Cycle number	5
Temperature	16.8 °C
Humidity	52%

TABLE III
EXPERIMENTAL CONDITIONS OF LOAD AMPLITUDE TEST
WITH INCREASING AMPLITUDE

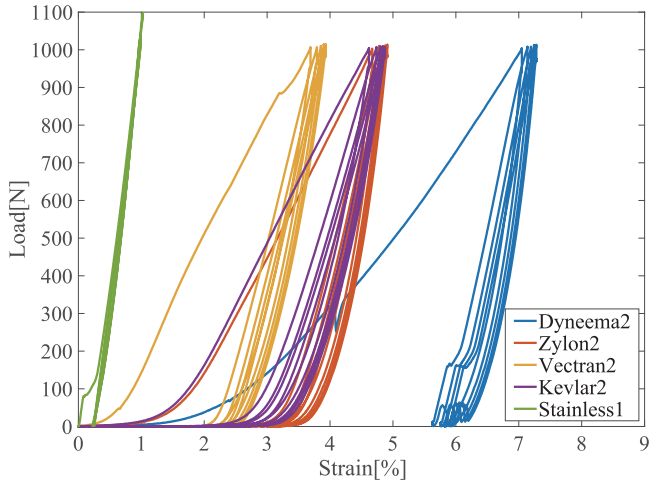|	
Frequency of load	1 Hz
Maximum load	Increment by 98.1 N each cycle
Minimum load	5 N
Cycle number	5
Temperature	17.1 °C
Humidity	28%

Fig. 3.   Results of the cyclic tensile tests.

Fig. 4.   Results of the load amplitude test.

speed and a maximum tension of 1000 N. A tensile tester (AG-I Shimadzu.co, maximum load of 100 kN) was used. Table II presents the experimental conditions. We performed the test on one sample of each rope. The initial length of test rope was determined through the following the tensile test procedure:

1) The distance between the two holding grips of the tensile tester was set to about 100 mm
2) Both ends of the test rope were fixed with the holding grips.
3) In order to straighten the test rope, the upper holding grip was moved up and down while keeping the tension within the range of 5 N or less.
4) The distance between the gripping tools at that time was taken as the initial length of the rope.
5) The tensile test was then carried out.

Fig. 3 shows the tension-strain curve of the test. The strain is defined as the elongation divided by the initial length. In the synthetic fiber ropes, a large plastic strain of more than 1% remained after the first loading and unloading, especially, that of Dyneema2 (about 5.5%). However, in the second and subsequent loadings and unloadings, the increase in plastic strain reduced to about 0.1%. This is sufficiently small to be absorbed by elastic elongation and a tensioner, because cable-pulley servo systems must have the tensioner to prevent rope slack. The plasticity of synthetic fiber ropes preserved the elongation at the maximum tension applied in the past. By contrast, the mechanical properties of Stainless1 showed extremely linear elasticity. Therefore, measurements described in the next section was not performed for Stainless1. The elastic coefficient of Stainless1 was $k_s = 1.37 \times 10^5$ N based on the slope of the line approximating the tension-strain curve using the least-squares method.
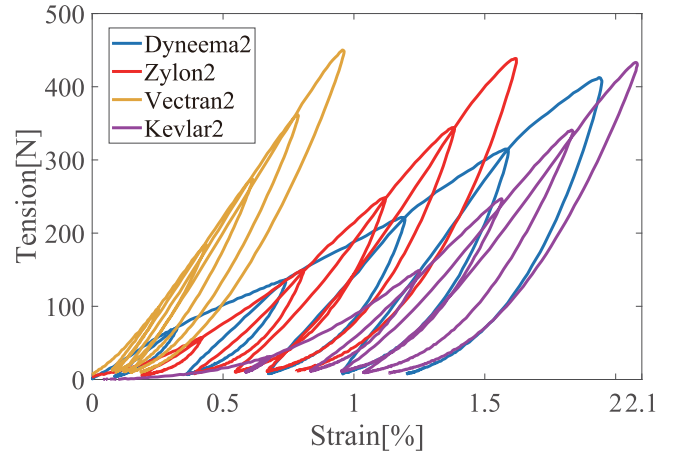
B. Elasto-Plasticity Experiments

A load amplitude test was carried out in which the peaks of cyclic load were gradually increased. A linear relationship was expected between both ε_p and ε_1 and the peaks of tension f_{peak}. The four synthetic fiber ropes in Table I were used. In order to reduce the elongation due to viscosity, a high tension speed is desirable, thus the test load was a 1 Hz haversine wave using a fatigue testing machine (SERVOPULSER Shimadzu.co, maximum load of 2 tf). The initial length of the test rope was determined in the same manner as for the cyclic load test described above. Table III shows the experimental conditions. We performed the experiment on one sample of each type of rope.

Fig. 4 shows tension-strain diagram. For all synthetic fiber ropes, the strain at the minimum tension (i.e., the plastic strain ε_p) increased with the maximum tension f_{peak}. Fig. 5 shows the fitting results for Dyneema2. The elastic strain ε_1 was obtained from (1), $\varepsilon_{\text{peak}}$, and ε_p. The distribution diagrams of the five peaks of tension versus both ε_1 and ε_p are given. The linear fitting lines of these two distribution diagrams are identified in the legend. The slopes of the two fitting lines give k_1 and k_p. k_p corresponds to the spring that is parallel to the ratchet element in Fig. 2, and k_1 corresponds to the leftmost spring in Figs. 2 and 1. The results of other synthetic fiber ropes were similarly approximated by straight line. Table IV summarizes the values of k_1 and k_p that were obtained by a linear approximation that satisfies (1) and (2). Therefore, Flory's model was confirmed to be applicable to the ropes. In this letter, "pre-stretch process" is defined as the preparatory process applying an initial force whose magnitude is larger than that of normal operation to a rope. This process lets us assume that the four-element model which is a linear model is applied to the synthetic fiber ropes.
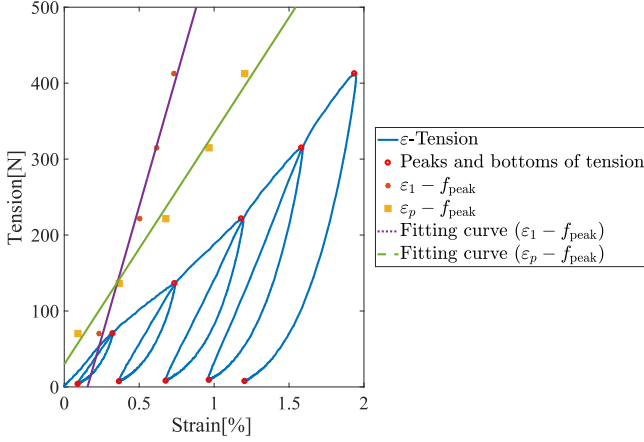
Fig. 5.   Peaks of tension proportional to elastic strain and plastic strain

TABLE IV
VALUES OF k_1 AND k_p

	$k_1 [\mathrm{N} \times 10^4]$	$k_p [\mathrm{N} \times 10^4]$
Dyneema2	6.89	3.04
Zylon2	6.19	6.51
Vectran2	5.94	31.5
Kevlar2	4.67	7.25

III. VISCO-ELASTICITY MEASUREMENT

Visco-elasticity measurements were conducted on synthetic fiber ropes subjected to prestretch process. The visco-elastic parameters k_1, c_2, k_3, and c_3 of four-element model in Fig. 1 were determined. To measure visco-elasticity, the tension relaxation was measured. When the tensile strain of the rope is instantaneously given and kept constant, the decrease in tension over time is called the tension relaxation. The visco-elasticity parameter was obtained by fitting the measured tension-time curve with the theoretical equation for the tension relaxation of the four-element model. The relationship between the total strain $\varepsilon(t)$ and tension $f_{\mathrm{model}}(t)$ of the four-element model is given by

$$f_{\mathrm{model}}(t) = k_1 \varepsilon_1 = c_2 \dot{\varepsilon}_2 = k_3 \varepsilon_3 + c_3 \dot{\varepsilon}_3, \qquad (3)$$

$$\varepsilon(t) = \varepsilon_1 + \varepsilon_2 + \varepsilon_3 = \varepsilon_0. \qquad (4)$$

The initial condition for the tension relaxation is given by

$$\varepsilon(0) = \varepsilon_1(0) = \varepsilon_0 \text{ and } \varepsilon_2(0) = \varepsilon_3(0) = 0. \qquad (5)$$

The tension $f_{\mathrm{model}}(t)$ is expressed as follows:

$$f_{\mathrm{model}}(t) = \frac{\varepsilon_0 k_1}{2B} \exp\left(-\frac{A+B}{D}t\right)(C+B)$$
$$- \frac{\varepsilon_0 k_1}{2B} \exp\left(-\frac{A-B}{D}t\right)(C-B)$$
$$A = c_2 k_1 + c_2 k_3 + c_3 k_1 \qquad (6)$$
$$B = \sqrt{(c_2 k_1 + c_2 k_3 + c_3 k_1)^2 - 4c_2 c_3 k_1 k_3}$$
$$C = c_2 k_1 - c_2 k_3 + c_3 k_1$$
$$D = 2 c_2 c_3$$

TABLE V
EXPERIMENTAL CONDITIONS OF THE TENSION RELAXATION TESTS

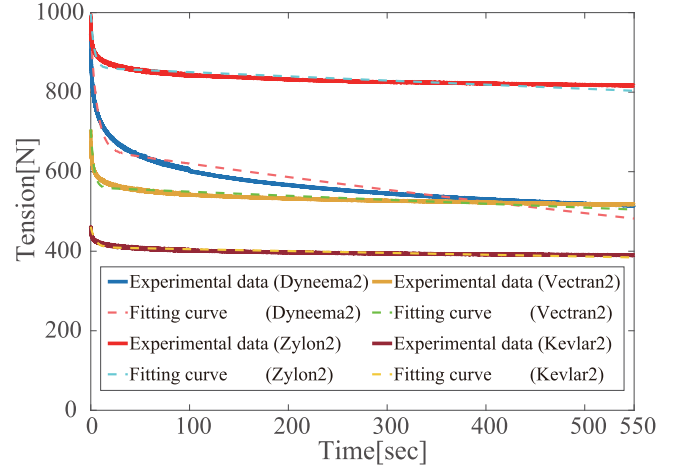|	
Constant elongation	1.5 mm
Tension for pre-stretch process	1000 N
Temperature (other than Kevlar2)	22.2 °C
Temperature (Kevlar2)	15.8 °C
Humidity (other than Kevlar2)	81%
Humidity (Kevlar2)	57%

Fig. 6.   Tension-time curves and fitting curves.

A tensile tester (AG-I Shimadzu.co) was used for the measurements. For the pre-stretch process, 1000 N were preloaded and immediately unloaded, and the tension was kept at 5 N or less for at least 10 minutes before the test. The delay was needed to allow the elongation caused by the retarded elasticity to recover. Table V shows the experimental conditions. Visco-elasticity measurement was performed on three specimens and they were similar trend. Values shown in Table V are representative of those obtained for the three specimens. After the prestretch process, the initial length of test rope was determined in the same manner as for the cyclic load test described above.

By minimizing the root mean square (RMS) of the measured tension f_{measure} and f_{model}, the time series of tension f_{measure} was fitted with (6). RMS is expressed as follow:

$$RMS = \sqrt{\frac{1}{N} \sum_{i=1}^{N} (f_{\mathrm{model}}(t_i) - f_{\mathrm{measure}}(t_i))^2} \qquad (7)$$

where N is the total number of measurement points, and t_i is the time of the sampling points. Fig. 6 shows measured tension and fitting curves.

Table VI gives the estimated visco-elastic parameters and RMS. The values of k_1 in Tables IV and VI the same meaning. Their values have the same order of magnitude, and the error is less than 29%. The RMS of each rope exhibited a small error compared to a applied tension on operation. A convergent tension at the end of the measurement was considered as the applied tension. The RMS value is only 4% of the applied tension even in the case of Dyneema2, which showed the largest RMS. RMS of each rope was evaluated as a small error by comparison with the applied tension. Convergence tension at the end of measurement was considered as applied tension. RMS is only 4% of the

TABLE VI
VISCO-ELASTIC PARAMETERS OF THE ROPES AND RMS

	k_1 [N × 10^4]	c_2 [N · s × 10^7]	k_3 [N × 10^5]	c_3 [N · s × 10^5]	RMS [N]
Dyneema2	7.29	9.02	1.65	15.7	17.7
Zylon2	7.48	51.1	4.76	19.4	8.15
Vectran2	5.08	21.3	1.94	7.65	7.89
Kevlar2	3.31	25.1	2.63	13.8	3.29

Fig. 7.   Long-distance cable-pulley system.

Fig. 8.   Analytical model of the testing machine.

TABLE VII
SYMBOLS IN FIG. 8

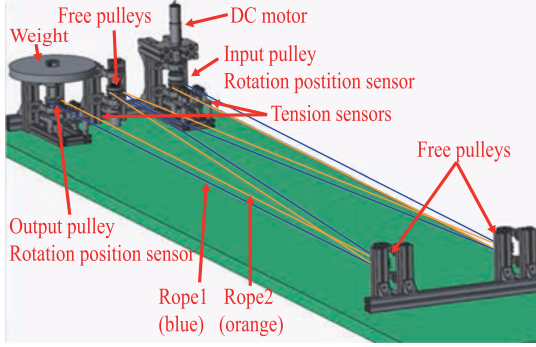| Name	Unit	
L	[m]	Length of test rope
k_1, k_3	[N]	Coefficients of elasticity
c_2, c_3	[N · s]	Coefficients of viscosity
I	[kg · mm²]	Moment of inertia
C	[kg · m² · s⁻¹]	Viscous resistance of pulleys
r_1, r_2	[mm]	Radius of pulley
θ	[deg]	Rotation angle of the input pulley
ϕ	[deg]	Rotation angle of the output pulley
l_i	[m]	Elongations of elements $i = 1, 2, 3$
f	[N]	Tension amplitude

applied tension even in the case of Dyneema2, which showed the largest RMS. Therefore, the visco-elasticity measurement was considered appropriate. The elastic coefficients k_1 of synthetic fiber ropes are about half that of Stainless1 $k_s = 1.37 \times 10^5$ N.

As suggested by (6), the tension began showing a exponential decay immediately after the test rope was placed under a constant strain, and the rate of decay gradually decreased. After sufficient time, the tension decayed at a constant speed. The exponential decrease in the tension ended more quickly for Vectran2 than for the other ropes. Therefore, considering that c_3 represents the retarded elasticity, c_3 for Vectran2 is less than that for other synthetic fiber ropes. In addition, the decay speed of the tension at 200 s after the start of the measurement was less for Zylon2, Vectran2 and Kevlar2 than for Dyneema2. This indicates that Dyneema2 has low creep resistance. c_2 expresses the creep resistance of the rope, and c_2 of Dyneema2 was smaller than that of the other ropes by one order of magnitude.

IV. DYNAMIC RESPONSE OF THE TENDON-DRIVEN SERVO SYSTEM

A. Testing Machine and Experimental Procedure

A long-distance servo system exceeding 10 m in length is required to develop a long-reach robot arm for decommissioning work. We constructed a 15.2 m servo system with a cable-pulley drive system that was as long as possible. Fig. 7 shows the tendon-driven servo system. The input and output are the rotation angle of the pulleys. Since it is difficult to model relay pulleys in detail, we decided to ignore these in this letter without discussing it in detail. However, due to the limitation in area, three relay pulleys are included in the system. The model used to derive the transfer function of the testing machine is shown in Fig. 8. Table VII describes the symbols used in Fig. 8. The tension amplitude f was half the difference between the tensions of Rope 1 and Rope 2. Here, C denotes the viscous resistance of the pulleys of the testing machine. When the rope is not set
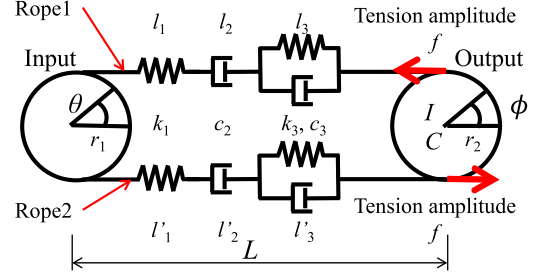
and the axis of the pulley is rotated freely by hand, the motion of the pulley axis is given by

$$I\ddot{\phi} + C\dot{\phi} = 0. \tag{8}$$

Where C was determined by measuring the attenuation of the angular velocity of the shaft over time. As inertial load, the weight was fixed such that the moment of the inertia of the test machine was $I = 2.84 \times 10^4 \mathrm{kg} \cdot \mathrm{mm}^2$ on the axis of the output pulley. The radii of pulleys, r_1 and r_2 are 25 mm and the length of the rope was $L = 15.2$ m.

The dynamic characteristics were measured by changing the rotation angle of the input pulley with a sine wave and measuring the response of the rotation angle of the output pulley. The input pulley was driven by a 150 W DC motor (301830, MAXON MOTOR), and the rotation of the input pulley was transmitted to the output pulley by two antagonistic ropes. The angles of the input and output pulleys were measured with a position sensor (E6B2-CWZ1X, Omron.co) with a resolution of 0.18 deg. The rope tension was measured at a total of four points near the input and output pulleys. In order to suppress the total length of the testing machine, Rope 1 and Rope 2 pass each passed through three shaft, as shown in Fig. 7. Each of the three shafts had two pulleys that rotated freely, and the two antagonistic ropes were wound separately. Therefore, on a free pulley, the two ropes did not slide, and the rope and pulley did not slip. For the rope used for the measurement, a tension of 490 N or more was preliminarily added to the test rope as a prestretch process. The averaged tension was varied from about 49 N to about 392 N in increments of about 49 N, and the measurement was carried out at each tension value. The input sine wave amplitude was 4.5 deg and the input frequency was swept from 0.1 Hz to 6.0 Hz. Measurement of the frequency response was performed three times with the same average tension. All measurements of one kind of rope were performed on one specimen.
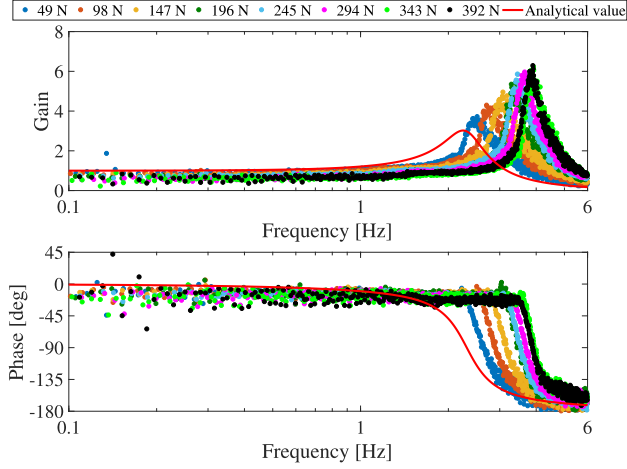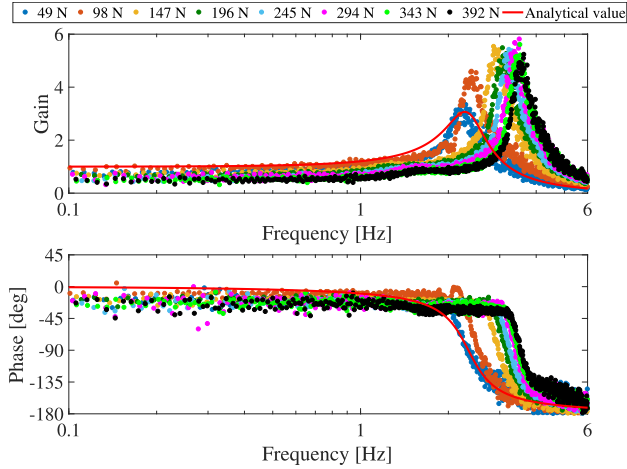
Fig. 9.   Frequency response with Dyneema2.

Fig. 11.   Frequency response with Vectran2.

Fig. 10.   Frequency response with Zylon2.

Fig. 12.   Frequency response with Kevlar2.

B. Experimental Results

A Bode diagram was obtained with a Fourier-transform of the input and output rotation angles. The results of the four ropes are shown in Figs. 9–13, and the legend indicates how the averaged tension was changed in eight ways. In all results, one resonance point was confirmed. The gain reached its maximum value at the resonance point, and the phase reversed before and after the resonance point. In addition, the gain on the high-frequency side of the resonance point decreased at −40 dB/deg. The resonance point shifted to the high-frequency side for all ropes with an increase in the averaged tension. However, it stopped shifting at around 294 N. In addition, the magnitude of the gain at the resonance point also changed along with the averaged tension. For Stainless1 and Dyneema2, the maximum gain increased with the averaged tension. For Zylon2, however, the maximum gain did not increase but converged to a certain value with increased averaged tension. For Vectran2 and Kevlar2, the maximum gain decreased by increasing the averaged tension.

Figs. 14 and 15 compare the results of different ropes with the same averaged tension. The resonance frequency of Vectran2 or Kevlar2 smallest and that of Dyneema2 is always the highest. The gain of Vectran2 at the resonance point was always the
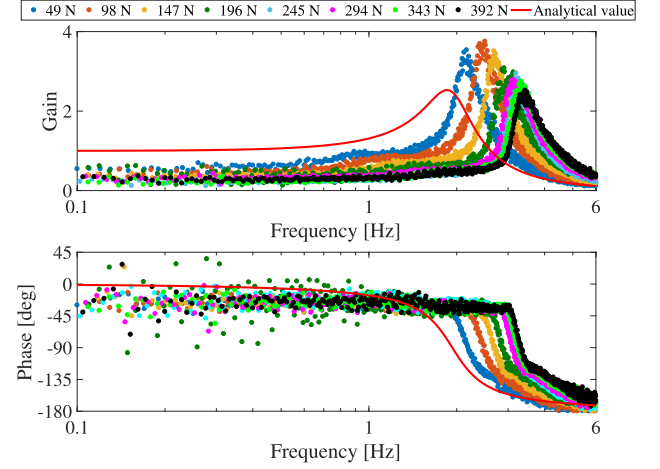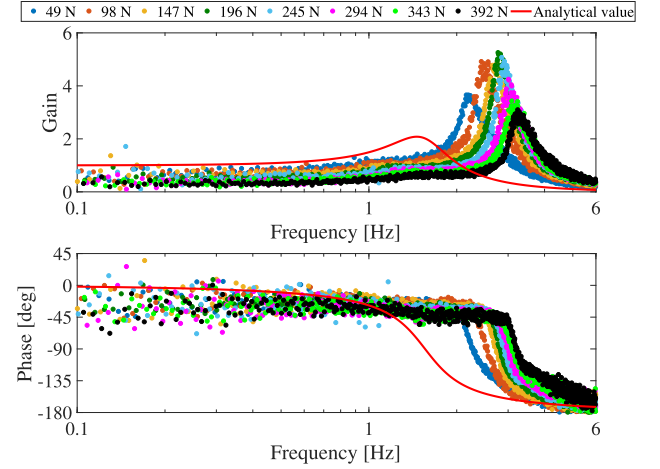
smallest, and that of Stainless1 was the largest. Dyneema2 and Zylon2 had about the same maximum gain.

The transfer function was obtained from the model of the testing machine shown in Fig. 8. The motion of the output pulley is given by

$$I\ddot{\phi} + C\dot{\phi} = 2r_2 f. \tag{9}$$

In Fig. 8, Rope 1 and Rope 2 are antagonistic. The elongation and tension of Rope 1 are given by (10) and those for Rope 2 are given by (11). In (11), replacing $l'_i = -l''_i$ is isomorphic to (10).

$$l_1 + l_2 + l_3 = r_1\theta - r_2\phi$$
$$f = k_1 l_1 = c_2 \dot{l_2} = k_3 l_3 + c_3 \dot{l_3} \tag{10}$$

$$l'_1 + l'_2 + l'_3 = -r_1\theta + r_2\phi$$
$$f = k_1 l'_1 = c_2 \dot{l'_2} = k_3 l'_3 + c_3 \dot{l'_3} \tag{11}$$

When the Laplace transform is performed on (9) and (10), the transfer function $G_{\text{VE}}(s)$ is given by

$$G_{\text{VE}}(s) = \frac{\mathcal{L}[\phi]}{\mathcal{L}[\theta]} = \frac{r_1}{\frac{Is^2 + Cs}{2r_2} \cdot \left(\frac{1}{k_1} + \frac{1}{c_2 s} + \frac{1}{k_3 + c_3 s}\right) + r_2} \tag{12}$$
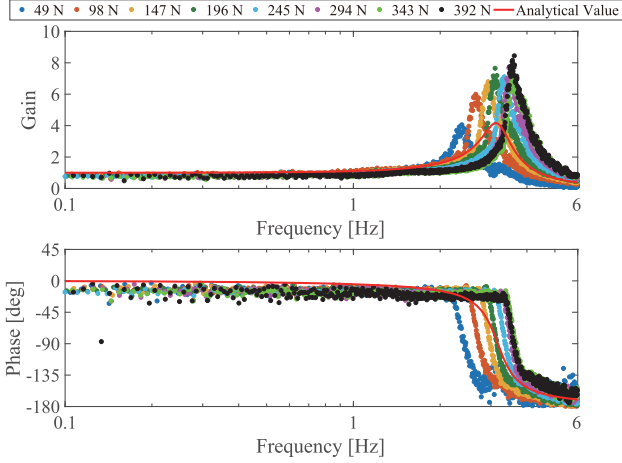
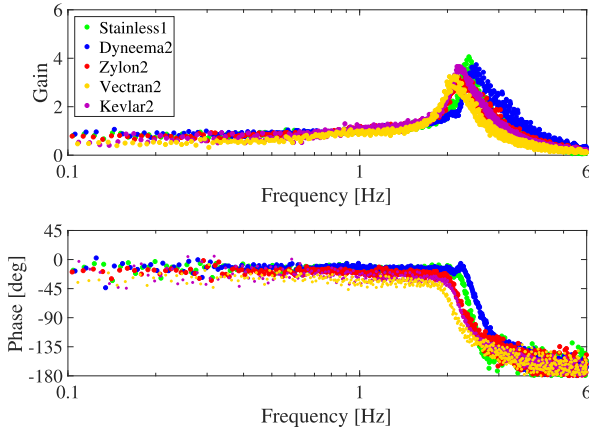Fig. 13.   Frequency response with Stainless1.

Fig. 14.   Frequency response when tension was 49 N.
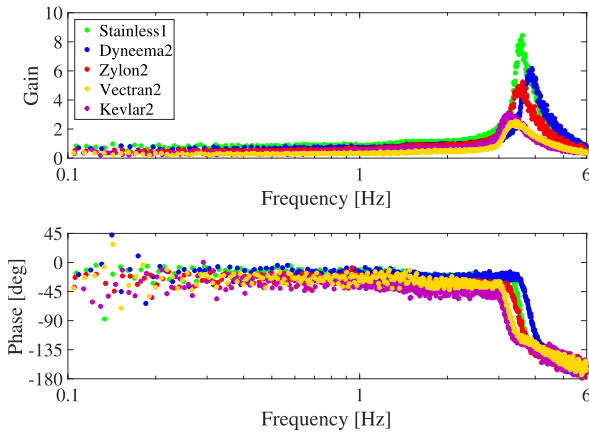

Fig. 15.   Frequency response when tension was 392 N.

Because Stainless1 is regarded as an elastic body, only the element of k_1 out of k_1, c_2, k_3, and c_3 was considered to obtain the transfer function $G_E(s)$, as shown in (13). The values of other elements were extremely large, and elongation of them did not occur.

$$G_E(s) = \frac{\mathcal{L}[\phi]}{\mathcal{L}[\theta]} = \frac{r_1}{\frac{Is^2 + Cs}{2r_2 k_1} + r_2}. \tag{13}$$

The transfer function into which the parameters for the mechanical properties were substituted was compared with the measured dynamic characteristics. For the four kinds of synthetic fiber ropes, the values in Table VI and (12) were used. For Stainless1, the value of $k_s = 1.37 \times 10^5$ N obtained from the cyclic tensile test and (13) was used. The obtained transfer functions are shown in Figs. 9–13 as legend "Analytical value". The transfer functions do not completely match the actual measured dynamic characteristics of the testing machine, but the frequencies of the resonance point and the maximum gains were of the same order of magnitude.

V. DISCUSSION

The dynamic characteristics were measured by using a long-distance cable-pulley system with four kinds of synthetic fiber ropes and Stainless1. The results show that the servo system is close to a second-order lag system regardless of the rope used. The frequency of the resonance point of the servo mechanism was between 2 and 4 Hz for any type of rope. This means that synthetic fiber ropes can drive the servo mechanism in the same range of frequency as the stainless steel wire rope with the same diameter, considering the servo mechanism is driven in a bandwidth lower than the resonance point to avoid intensifying the vibrations.

As the averaged tension increased, the resonance point shifted to the high-frequency side for all ropes. This is thought to be due to the nonlinearity of the elastic coefficient. As shown in Fig. 3, the tension-strain diagram of the rope draws a downwardly convex curve, and the elastic coefficient increases with the averaged tension and the strain. However, while the testing machine was running, the elastic coefficient was assumed to be constant. To estimate the maximum amount of change in rope strain while the testing machine was running, if the position gain was assumed to be 10 and calculated from the length of rope and radius of pulleys, the amount of change in strain is as small as $\pm 0.13\%$. Therefore, the change in elastic coefficient was also assumed to be small while the servo system was driven. It is thus reasonable to treat the model in this letter as having a constant elastic coefficient.

If the rope is a simple elastic body and the servo system is a second-order lag system, the maximum gain never decreases as the resonance point shifts to the higher side. However, the gain clearly declined for Vectran2 and Kevlar2 as the resonance point shifted. This may be because the visco-elasticity of synthetic fiber ropes is close to elastic, but the viscous damping and structural damping of Vectran2 and Kevlar2 are greater than those of the others.

Both the transfer function and the Bode diagram are close to the second-order lag system and the resonance point and the gain have the same order of magnitude. The model in Fig. 8 conforms with reality, and thus can be used to model the dynamic characteristics of a tendon-driven mechanism.

All synthetic fiber ropes decreased the gain of the servo system relative to the stainless-steel wire rope. The large difference in gain at the resonance point may be due to the damping derived from the viscosity and plasticity of synthetic fiber ropes. A tendon-driven servo system that needs to drive a large amount of inertia compared with the stiffness of the joint, such as a long-reach robot arm, vibrates easily with long settling time. Thus, an additional damper is often placed on the joint to shorten the settling time. If the vibration can be sufficiently suppressed

without an additional damper by using a synthetic fiber rope, the structure will be lighter. Synthetic fiber ropes thus seem more suitable than stainless wire ropes for such applications.

VI. Conclusion

In this letter, we investigate the frequency response of a long-distance cable-pulley system using synthetic fiber ropes. Four synthetic fiber ropes braided with the same method and a stainless-steel wire rope of the same diameter were compared. The results are summarized as follows:

1) The Flory's model was confirmed to be applicable to different types of synthetic fiber rope with a diameter of 2 mm. This model can be used to quantitatively compare different types of synthetic fiber ropes.

2) The elastic coefficient of ropes made with UHPE, PBO, Polyarylate, and Aramid are about half of the elastic coefficient of the stainless-steel wire rope. However, in the testing machine, frequency responses were of the same order in any rope, which means that it can be driven in the same bandwidth.

3) The dynamic characteristics of the mechanism were confirmed as related to the visco-elasticity of the rope. In particular, the synthetic fiber ropes showed lower gain in the tendon-driven servo mechanism. This is considered to be due to viscous and structural damping.

In the future, we shall evaluate other types of rope of varying diameters, fibers, and braiding methods. Insofar as environmental conditions affect the mechanical properties of rope (e.g., humidity, temperature, and radiation), this must also be investigated. Moreover, the precision and scalability of the model for synthetic fiber rope need to be improved. Therefore, we shall consider the nonlinearity of elasticity, mass or sagging rope, friction on guide elements, variation of properties, and the influence of the method of preloading on model errors. Finally, we shall investigate other physical properties, such as creep over the long term and friction durability, in order to provide design guidelines for synthetic fiber rope.

Acknowledgment

References

[1] TOYOBO, "IZABAS properties." [Online]. Available: http://www.toyobo-global.com/seihin/dn/izanas/iz_product/features.html, Accessed on: Aug. 30, 2017.

[2] TOYOBO, "Technical data sheet of Zylon." [Online]. Available: http://www.toyobo-global.com/seihin/kc/pbo/zylon-p/bussei-p/technical.pdf, Accessed on: Aug. 30, 2017.

[3] KURARAY, "Basic physical properties." [Online]. Available: http://www.kuraray.co.jp/vectran/en/tokutyou/s01.html, Accessed on: Aug. 30, 2017.

[4] W. Kraus, A. Spiller, and A. Pott, "Energy efficiency of cable-driven parallel robots," in *Proc. 2016 IEEE Int. Conf. Robot. Autom.*, Stockholm, 2016, pp. 894–901.

[5] S. Kitano, S. Hirose, A. Horigome, and G. Endo, "TITAN-XIII: sprawling-type quadruped robot with ability of fast and energy-efficient walking," *ROBOMECH J.*, vol. 3, no. 1, pp. 1–8, 2016.

[6] T. Kozuki *et al.*, "Muscle-tendon complex control by tension controlled musclei and non-linear spring ligament for real world musculoskeletal body simulator Kenshiro," in *Proc. 5th IEEE RAS/EMBS Int. Conf. Biomed. Robot. Biomechatronics*, Aug. 2014, pp. 875–880.

[7] A. Horigome, H. Yamada, G. Endo, S. Sen, S. Hirose, and E. F. Fukushima, "Development of a coupled tendon-driven 3D multi-joint manipulator," in *Proc. 2014 IEEE Int. Conf. Robot. Autom.*, pp. 5915–5920.

[8] V. Sry, Y. Mizutani, G. Endo, Y. Suzuki, and A. Todoroki, "Consecutive impact loading and preloading effect on stiffness of woven synthetic-fiber rope," *J. Textile Sci. Technol.*, vol. 3, no. 1, pp. 1–16, 2017.

[9] W. Kraus, V. Schmidt, P. Rajendra, and A. Pott, "System identification and cable force control for a cable-driven parallel robot with industrial servo drives," in *Proc. 2014 IEEE Int. Conf. Robot. Autom.*, Hong Kong, 2014, pp. 5921–5926.

[10] P. Miermeister, W. Kraus, T. Lan, and A. Pott, "An elastic cable model for cable-driven parallel robots including hysteresis effects," in *Cable-Driven Parallel Robots*. Berlin, Germany: Springer-Verlag, 2015, pp. 17–28.

[11] A. Mazumdar *et al.*, "Synthetic fiber capstan drives for highly efficient, torque controlled, robotic applications," *IEEE Robot. Autom. Lett.*, vol. 2, no. 2, pp. 554–561, Apr. 2017.

[12] R. A. Schapery, "Nonlinear viscoelastic and viscoplastic constitutive equations based on thermodynamics," *Mech. Time-Dependent Mater.*, vol. 1, no. 2, pp. 209–240, 1997

[13] E. Chailleux, and P. Davies, "Modeling the non-linear viscoelastic and viscoplastic behaviour of Aramid fibre yarns," *Mech. Time-Dependent Mater.*, vol. 7, no. 3, pp. 291–303, 2003.

[14] P. Sherman, *Industrial Rheology: With Particular Reference to Foods, Pharmaceuticals, and Cosmetics*. London, U.K.: Academic Press, 1970, p. 18.

[15] J. F. Flory, V. Ahjem, and S. J. Banfield, "A new method of testing for change-in-length properties of large fiber-rope deepwater mooring lines," in *Proc. Offshore Technol. Conf.*, Apr. 30–May 3, 2001, pp. 1087–1096.